PHYSICAL REVIEW B

SOLID STATE

THIRD SERIES, VOL. 6, NO. 4 15 AUGUST 1972

L-Shell Soft-X-Ray Appearance-Potential Spectra of the $3d$ Transition Metals*

Robert L. Park and J. E. Houston
Sandia Laboratories, Albuquerque, New Mexico 87115
(Received 25 February 1972)

We have obtained L-shell appearance-potential spectra for clean surfaces of the $3d$ transition metals: Sc, Ti, V, Cr, Mn, Fe, Co, and Ni. Spin-orbit splittings determined from these spectra are in excellent agreement with tabulated x-ray values. In all cases, however, the absolute binding energies are lower than the tabulated values, presumably as a result of the reduced coordination for surface atoms. The L_3/L_2 intensity ratios show a systematic variation with Z, approaching the expected statistical weighting of 2 only for a nearly empty (Sc) or nearly filled (Co and Ni) $3d$ band. It is less than 2 for all intermediate Z's with a minimum value of approximately 1 at Cr. The L_3, L_2 peak widths decrease with Z corresponding to the filling of the $3d$ band. The L_1 width, which is determined primarily by Auger lifetime broadening rather than the density of conduction-band states, exhibits a systematic decrease for $Z > 24$ in contrast to theoretical predictions.

I. INTRODUCTION

The importance of the $3d$ transition metals to technology has stimulated experimental studies of their electronic structure by a variety of deep-hole probes such as x-ray photoelectron spectroscopy, soft-x-ray emission and absorption spectroscopy, electron-excited Auger spectroscopy, etc. Because of uncertainties resulting from differences between the various probes and in the details of the experimental techniques, however, information on systematic changes in electronic structure with Z can be reliably extracted only from studies of the complete series by a single technique using a single instrument. Filled-band studies of this sort include L_2, L_3 x-ray emission-band spectra of elements 20–29[1] and $M_{2,3}$ emission-band spectra of elements 22–29.[2] Ultraviolet-photoelectron valence-band spectra have been obtained by Eastman[3] for elements 21–28. In the present paper we report the results of a systematic study of the L-shell spectra of elements 21–28 by soft-x-ray appearance-potential spectroscopy which is an empty-band (absorption) probe.

The soft-x-ray appearance-potential technique[4] depends on the fact that the total x-ray emission of electron-bombarded surface, plotted as a function of incident electron energy, exhibits distinct structure corresponding to the core-level-excitation probabilities superimposed on a bremsstrahlung background. The excitation edges can be sensitively detected in the derivative of the photocurrent from any metal surface exposed to x rays from the bombarded sample. The shape of the edges is related to the density of conduction-band states. The results are therefore equivalent to those obtained by the characteristic isochromat technique.[5–7] In both techniques, the resolution is ultimately limited only by the spread in incident electron energies. The advantage of the appearance-potential technique is its simplicity.

It should be emphasized that, owing to the small mean free path for inelastic scattering of electrons in the energy range below 1000 eV, appearance-potential spectroscopy samples only the outermost few atomic layers. It is not clear therefore to what extent agreement should be expected with calculations or measurements which claim validity only for bulk atoms.

II. EXPERIMENTAL

Ultrahigh-purity polycrystalline samples[8] of Ti, V, Cr, Fe, Co, and Ni were prepared in the form of disks 12 mm in diam by 3 mm thick. The flat surfaces were mechanically polished, ultrasonically agitated, and degreased in acetone before being placed in the vacuum system. A carrousel multiple-sample holder consisting of six molybdenum

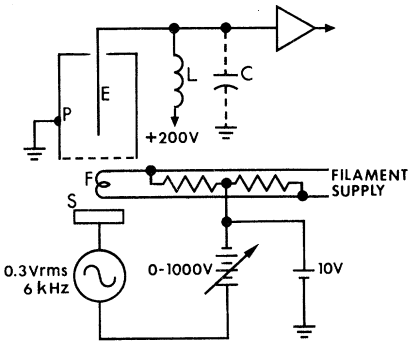

FIG. 1. Schematic diagram of the soft-x-ray appearance-potential spectrometer. The sample S is bombarded by electrons from a tungsten filament F. X rays from the sample pass through the grid and impinge on the walls of the photocathode can P producing photoelectrons which are collected on the electrode E. That portion of the collector current which varies at the modulation frequency is selected by a tuned circuit.

pans was used to rotate the samples from the measurement position to other stations for cleaning by electron-bombardment heating of the sample pans and argon-ion sputtering. In addition, the samples could be positioned under Mn and Sc evaporators. These two metals could not be obtained in high-purity specimens suitable for direct study. Consequently, small high-purity samples were placed in directly heated tungsten coils and evaporated onto the other six samples which served as substrates subsequent to taking the spectra of their clean surfaces. In this way, the spectra of all eight metals could be obtained without breaking the vacuum.

The surfaces were subjected to repeated cycling of sputtering and high-temperature outgassing to remove all traces of impurities such as C, O, and Ca. Some material was transferred from one sample to another during sputtering and traces of other $3d$ metals were usually detectable on the "clean" surfaces; however, the amounts were much too small to measurably influence the substrate spectra.

Chamber pressures during the measurements were $< 10^{-9}$ Torr. In addition, the samples were maintained at several hundred degrees centigrade. No contamination could be detected over periods much longer than the time required to obtain a spectrum.

The essential features of the apparatus for the actual measurements of the spectra[4] are shown schematically in Fig. 1. Electrons emitted thermionically from a tungsten filament F are accelerated and produce soft x rays upon colliding with the sample S. The filament is in the form of a heavy ribbon of ultrapure tungsten with the narrow edge facing the sample. The ribbon is thinned slightly over a short region to localize the emission. The potential drop across the emitting portion is at most a few tenths of a volt.

Most of the x rays from the sample pass through a grid and strike the walls of the stainless-steel can P that serves as a photocathode. Photoelectrons from the walls are collected on a positively biased coaxial collector wire E. The filament is biased a few volts above the grid, which is at ground potential, to prevent filament electrons from reaching the collector. The collector current is therefore proportional to the total x-ray emission of the sample.

To obtain the approximate derivative of the photocurrent as a function of incident electron energy, a sinusoidal oscillation is superimposed on the accelerating potential. A tuned circuit composed of a high-Q inductor L in parallel with the distributed capacitance C of the collector circuit selects that portion of the collector current which varies at the modulation frequency. For weak signals it is advantageous to use a phase-lock amplifier. In the measurements reported here, the amplitude of the oscillation was fixed at 0.3 V rms. The oscillation frequency was approximately 6 kHz. Since the bremsstrahlung background is a relatively slowly varying function of incident electron energy, the output is approximately the derivative of the core-level-excitation probabilities superimposed on a nearly constant background.

The spectra shown here are all direct recorder tracings of the amplitude of the alternating component of the collector current versus the potential applied between the filament and sample. The X-Y plotter was calibrated to an accuracy of ± 0.1 V.

III. L-SHELL BINDING ENERGIES

The measurement of energy-level differences is simpler and more precise than the measurement of absolute binding energies and is, moreover, relatively unaffected by the distribution of valence electrons. The determination of the spin-orbit splitting $(L_3\text{-}L_2)$ is, however, complicated by the fact that L_2 structure may be distorted by the extended structure above the L_3 edge. The problem is serious only for the low-Z end of the series (Sc, Ti, and V) where the splitting is small and the threshold peaks are broader, as seen in Figs. 2–9 showing the $2p$ spectrum of the entire series.

The decomposition of the measured spectra into separate L_3 and L_2 contributions should be possible if the spectra differ only in their relative amplitudes, i.e.,

$$L_{2,3}(E) = L_3(E) + L_3(E - \Delta E)/\alpha \,, \qquad (1)$$

where α is the ratio of intensities, and ΔE is the

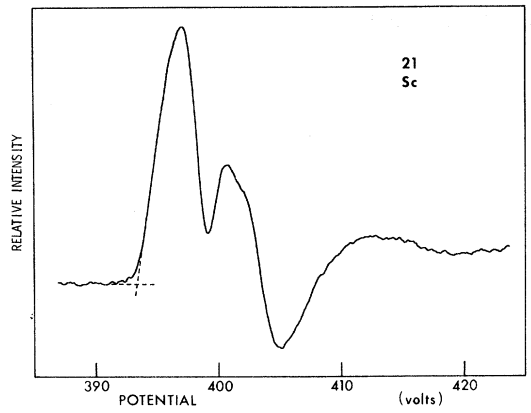

FIG. 2. $2p$ spectrum of Sc. The ordinate is approximately the derivative of the total x-ray emission. The $2p_{3/2}(L_3)$ threshold is taken as the intersection of the dashed lines. A 5.0-eV correction for filament work function, etc., must be added to convert to binding energy.

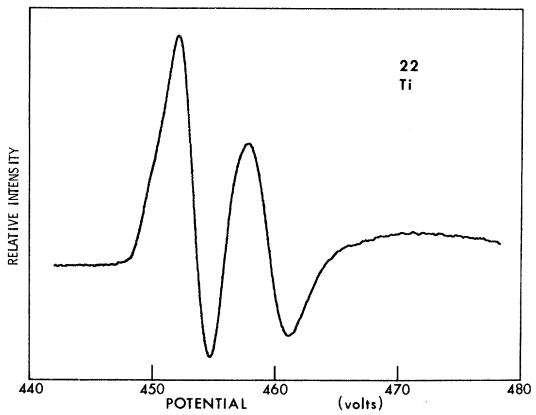

FIG. 3. $2p$ spectrum of Ti.

spin-orbit splitting. In fact, however, a broadening of the L_2 features relative to the L_3 results from the lifetime effects of the $L_3 \rightarrow L_2$ Coster-Kronig transition, but this is presumably not an important transition for the $3d$ series, [9] and the effect should be small. Calculations were therefore made to determine the values of α and ΔE which most nearly removed all remnants of the L_2 structure when the second term of Eq. (1) was subtracted from the total spectrum. The spin-orbit splittings determined in this way are compared to those tabulated by Bearden and Burr[10] in Table I. The agreement is within the probable error for most of the series. From the structure remaining in the decomposed spectra following the minimization procedure it was evident that there were some differences in the L_3 and L_2 shapes.

There is, of course, no problem with the $2p$ spectrum (L_3, L_2) overlapping the $2s$ (L_1). However, as expected from fluorescent-yield calculations, [9] the L_1 peaks are relatively weak and broad compared to the L_3 and L_2. This is seen in Fig. 10 which shows the complete L spectrum of iron. The measured L_3-L_1 separations are also listed in Table I and compared with the values tabulated in Ref. 10.

We also determined the binding energies of the core levels. We take the binding energy to be the minimum energy required to excite an electron from a given level to an available state above the Fermi energy. Therefore, to convert from the applied potential U to the energy of the incident electrons relative to the Fermi energy, it is necessary to multiply U by the electronic charge and add the work function of the filament $e\varphi$. [11] We have used a value of 4.5 eV for the thermionic work function of the tungsten emitter. [12] It is, of course, only necessary to make an absolute determination of the threshold energy E_B of one of the levels. The L_3 level, which was used by Siegbahn as a fundamental reference level for most of the periodic table, [13] was selected for obvious reasons. To make this determination directly from the recorder plots, it is necessary to add an additional correction $\frac{1}{2}e\Delta U$ corresponding approximately to half the peak-to-peak modulation of the sample po-

TABLE I. Measured energy-level differences (eV) compared to tabulated x-ray values.

	L_3-L_2		L_3-L_1	
	Park and Houston	Bearden and Burr[a]	Park and Houston	Bearden and Burr[a]
21 Sc	4.7 ± 0.1	4.50 ± 0.17	98.0 ± 0.4	
22 Ti	5.9 ± 0.1	5.98 ± 0.05	105.0 ± 0.4	
23 V	7.4 ± 0.1	7.55 ± 0.06	113.2 ± 0.4	114.35 ± 2.53
24 Cr	8.7 ± 0.1	9.21 ± 0.05	120.1 ± 0.4	121.95 ± 0.70
25 Mn	10.6 ± 0.1	11.10 ± 0.06	127.7 ± 0.4	129.72 ± 0.84
26 Fe	13.0 ± 0.1	13.00 ± 0.04	136.4 ± 0.4	137.96 ± 1.06
27 Co	15.1 ± 0.1	15.01 ± 0.05	145.7 ± 0.4	147.30 ± 1.22
28 Ni	17.3 ± 0.1	17.25 ± 0.05	156.5 ± 0.4	154.34 ± 0.72

[a]Reference 10.

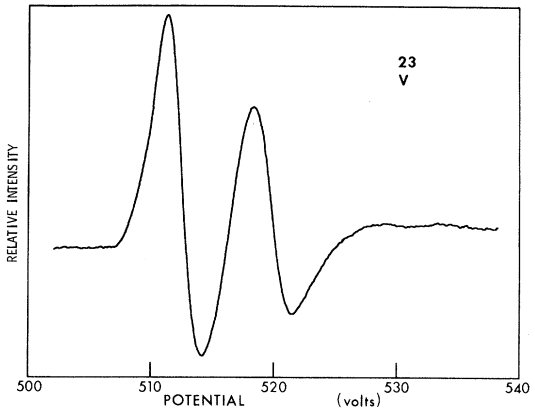

FIG. 4. $2p$ spectrum of V.

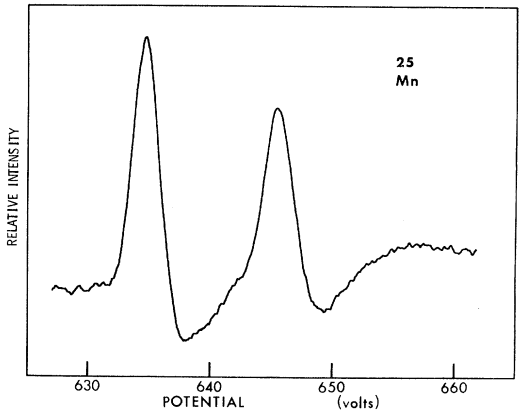

FIG. 6. $2p$ spectrum of Mn.

tential:

$$E_B = eU_T + e\varphi\,(4.5\text{ eV}) + \tfrac{1}{2}e\Delta U\,(0.5\text{ eV})\,. \qquad (2)$$

A slight correction to take account of the average thermal energy of the emitted electrons kT is included in the 0.5 eV. In these measurements, the thermal spread was less than the modulation amplitude and resulted mostly in a rounding of the thresholds, which otherwise should have been quite sharp. The L_3 thresholds were therefore determined as indicated by the intersection of the dashed lines in the $2p$ spectrum of Sc (Fig. 2). The total correction used to convert from the threshold potential U_T to the binding energy E_B was 5.0 eV. The binding energies determined in this way are given in Table II and compared to the values tabulated by Bearden and Burr.[14] It will be noticed that the appearance-potential results in every case are lower than the tabulated values, although the probable errors overlap in some cases.

IV. L_3/L_2 INTENSITY RATIOS

On the basis of simple theory, one would expect the relative intensities of the L_3 and L_2 spectra to be given by the statistical weighting $2j+1$. This predicts an L_3/L_2 intensity ratio of 2, but it is clear from even a cursory inspection of the raw spectra in Figs. 2–9 that this is not generally the case.

A precise determination of the intensity ratios involves integration under the positive threshold peaks since, as we pointed out above, there is some broadening of the L_2 features relative to the L_3 as a consequence of $L_3 \rightarrow L_2$ Coster-Kronig transitions. The accuracy of this integration depends on the extent to which the measured L_2 spectrum is distorted by the following structure of the L_3 spectrum. For $Z \geq 24$, this distortion is not serious. For $Z < 24$, the threshold-peak width is determined almost entirely by the width of the unfilled $3d$ band, as we will see in Sec. V, and the relative peak heights should be a good approximation to the relative intensities. We have therefore taken the value of α in Eq. (1) which minimized the following structure of the decomposed spectra to be a reasonable measure of the intensity ratio for $Z < 24$. The results are plotted in Fig. 11.

The intensity ratio varies systematically across

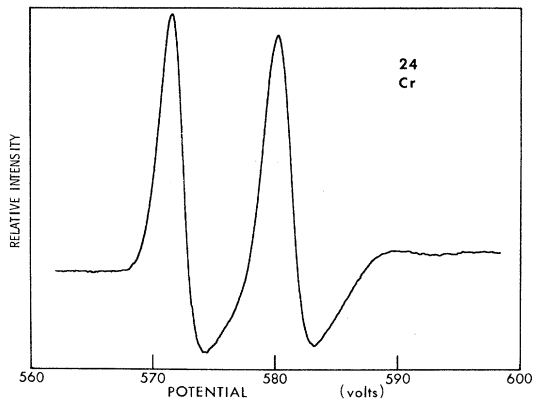

FIG. 5. $2p$ spectrum of Cr.

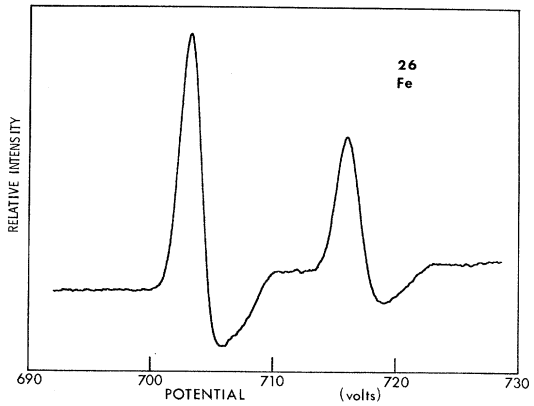

FIG. 7. $2p$ spectrum of Fe.

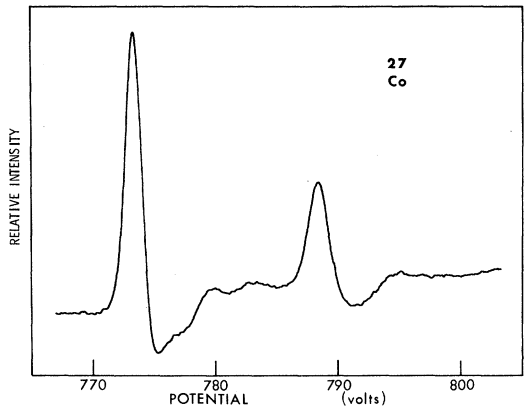

FIG. 8. $2p$ spectrum of Co.

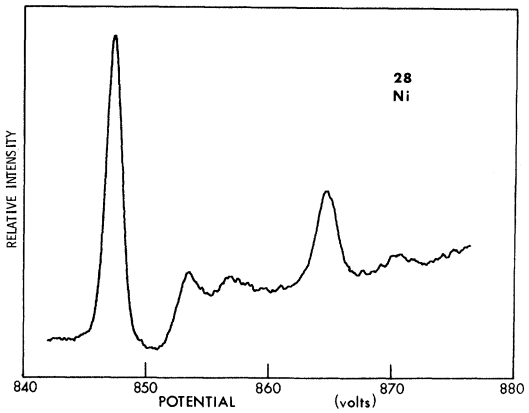

FIG. 9. $2p$ spectrum of Ni.

the series with a distinct minimum at Cr. Deviation from the statistical weighting of 2 implies either an anomaly in the excitation probabilities or j-dependent selection rules for the radiative decay of $2p$ holes. The first of these possibilities has been eliminated for Cr by comparing the intensity ratio measured by soft-x-ray appearance-potential spectroscopy with that obtained by Auger-electron appearance-potential spectroscopy.[15] The latter is essentially just the energy derivative of the secondary-electron-emission coefficient. Since the probability of a radiative decay is quite small, the Auger-electron appearance-potential spectrum should accurately reflect the relative excitation probabilities of the $2p$ levels regardless of differences in radiative-transition probabilities. The L_3/L_2 ratio for Cr in the Auger case was found to be almost exactly 2. We are forced to conclude therefore that, at least for chromium, $2p_{1/2}$ holes decay via radiative transitions with a greater probability than $2p_{3/2}$ holes. This point is discussed in greater detail in Ref. 15.

V. BAND MODEL

The total soft-x-ray emission from an electron-bombarded sample consists of the core-level-excitation probabilities superimposed on a smoothly increasing bremsstrahlung background. In the simple one-electron picture, assuming constant oscillator strengths, the excitation probabilities are proportional to the integral product of the densities of initial and final states. For our purposes, the initial states are the filled core levels which are to be emptied. The final states, on the other hand, must take into account all possible positions for the two electrons (incident and excited core electron) which are allowed by the conservation of energy as shown in Fig. 12.

The density of final states for two electrons is thus given by the self-convolution of the empty-state density for one electron $N(E)$, i.e.,

$$N_2(E) = \int_0^E N(E')\, N(E - E')\, dE' , \tag{3}$$

where the zero of energy is taken to be the Fermi level. Taking into account the finite width of the excited core level $\hbar/\tau$, where τ is the lifetime of a core hole, the transition probability above the threshold should go as

$$T(E) = \int_0^E \int_0^{E'} N(E'')\, N(E' - E'')\, dE'' \times N_c(E + E_B - E')\, dE' , \tag{4}$$

TABLE II. Measured L-shell electron-binding energies (eV) compared to tabulated x-ray values.

	L_3 ($2p_{3/2}$)		L_2 ($2p_{1/2}$)		L_1 ($2s$)	
	Park and Houston	Bearden and Burr[a]	Park and Houston	Bearden and Burr[a]	Park and Houston	Bearden and Burr[a]
21 Sc	398.4 ± 0.5	402.2 ± 0.4	403.1 ± 0.5	406.7 ± 0.4	496.4 ± 0.7	500.4 ± 0.4
22 Ti	453.4 ± 0.5	455.5 ± 0.4	459.3 ± 0.5	461.5 ± 0.4	558.4 ± 0.7	563.7 ± 0.4
23 V	512.6 ± 0.5	512.9 ± 0.3	520.0 ± 0.5	520.5 ± 0.3	625.8 ± 0.7	628.2 ± 0.4
24 Cr	574.0 ± 0.5	574.5 ± 0.3	582.7 ± 0.5	583.7 ± 0.3	694.1 ± 0.7	694.6 ± 0.4
25 Mn	638.5 ± 0.5	640.3 ± 0.4	649.1 ± 0.5	651.4 ± 0.4	766.2 ± 0.7	769.0 ± 0.4
26 Fe	706.3 ± 0.5	708.1 ± 0.9	719.3 ± 0.5	721.1 ± 0.9	842.7 ± 0.7	846.1 ± 0.4
27 Co	776.9 ± 0.5	778.6 ± 0.3	792.0 ± 0.5	793.6 ± 0.3	992.6 ± 0.7	925.6 ± 0.4
28 Ni	850.9 ± 0.5	854.7 ± 0.4	868.2 ± 0.5	871.9 ± 0.4	1007.4 ± 0.7	1008.1 ± 0.4

[a]Reference 14.

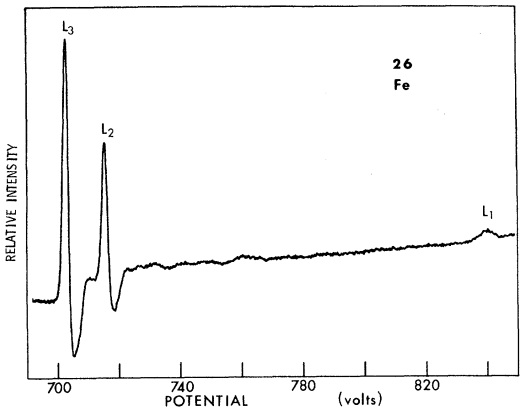

FIG. 10. Complete L spectrum of Fe indicating the relative weakness of the L_1 peak.

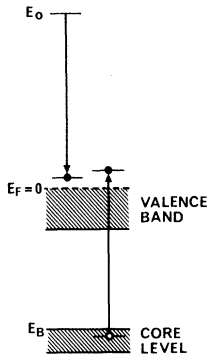

FIG. 12. Energy-level diagram of the excitation of a core level. The width of the excited core level is just $\hbar/\tau$, where τ is the lifetime of the core hole. All combinations of final positions of the incident and excited core electrons are possible which satisfy the conservation of energy.

where $N_c(E)$ is the state density function of the excited core level. If the lifetime of the core hole is sufficiently long, we can represent $N_c(E)$ by a δ function:

$$N_c(E) = n_c\,\delta(E - E_B)\,, \tag{5}$$

in which case the transition probability becomes

$$T(E) = n_c \int_0^E N(E')\,N(E - E')\,dE'\,. \tag{6}$$

Therefore, as long as we confine ourselves to excited core levels with sufficiently long lifetimes, the excitation probability is proportional to the self-convolution of the density of available states above the Fermi energy.[16] A qualitative idea of the shape of this function for a transition metal is given in Fig. 13. The solid curve (a) in Fig. 13 represents the density of states of a $3d$ transition metal. Although highly schematic, it does include the properties normally attributed to these materials, i. e., a sharp $3d$ band superimposed on a broad free-electron-like $4s$ band. In a simple rigid-band representation, the shape of the bands is fixed, and only the position of the Fermi level changes as the states are progressively filled with increasing Z.

The dotted curve (b) corresponds to Eq. (5) and is, to a first approximation, the shape one observes for the characteristic isochromat of a core level of a transition metal.[5-7] In the appearance-potential technique, however, we obtain the derivative of the transition probability which is represented in Fig. 13 by the dashed curve (c).

From this highly simplified representation, we expect that the appearance-potential spectrum of a given core level of a $3d$ transition metal will exhibit a positive threshold peak whose width is approximately equal to the width of the unfilled $3d$ band, followed by a negative-going dip. In the absence of the $4s$ band, the negative dip would equal the positive peak. The reduction of the negative

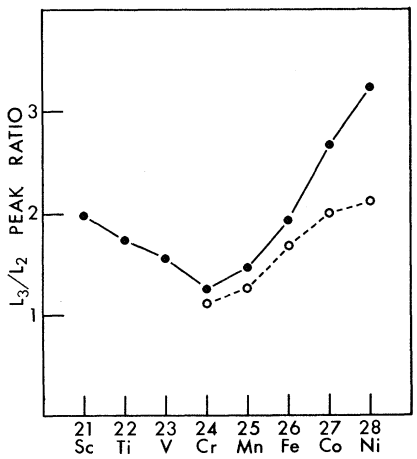

FIG. 11. L_3/L_2 intensity ratios. The open circles for Cr-Ni represent actual intensity ratios calculated by integrating under the peaks. The solid dots give the ratio of peak heights. For $Z < 24$ this should be a good approximation to the intensity ratio.

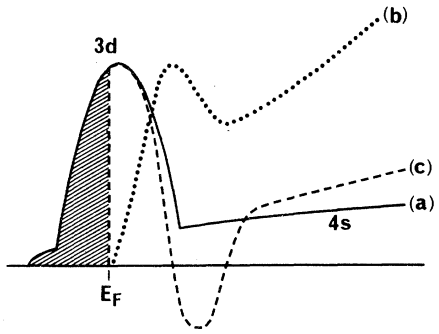

FIG. 13. Simplified schematic representation of the density of states of a $3d$ transition metal. (a) One-electron density of states. The states are occupied up to E_F. (b) Self-convolution of the density of unoccupied states (dotted curve). This is essentially the shape of the characteristic isochromat of a narrow core level. (c) Derivative of the self-convolution (dashed curve). This is the shape expected for the appearance-potential spectrum.

dip thus measures the relative contribution of the 4*s* states. The general trend of the 2*p* spectra in Figs. 2–9 clearly follows a rigid-band representation with the unoccupied 3*d* width decreasing with *Z* and the relative contribution of the 4*s* states increasing.

The measured width of the positive peak includes the effect of an instrument response function. To compare the observed spectra with theoretical calculations of the width of the unfilled 3*d* band, we have assumed that the threshold-peak widths measured at half-maximum are the quadratic sum of the intrinsic width and a 1-eV instrument response function which results primarily from the amplitude of the potential modulation. The corrected widths are plotted in Fig. 14 along with the widths of the unfilled *d* band calculated by Snow and Waber.[17] Although a great many energy-band calculations have been made in the past few years for individual 3*d* metals, Snow and Waber's augmented-plane-wave (APW) calculations, to our knowledge, constitute the only systematic treatment of the entire series.

The measured widths, corrected for instrument response, display the expected decreasing trend with *Z* and are in reasonable qualitative agreement with Snow and Waber's calculations. The agreement is worst for V and Cr. The Fe, Co, and Ni values all lie above the calculated widths, but if corrected for the lifetime broadening of the L_3 level (theoretical lifetime values[9] are indicated in Fig. 14 by *X*'s), they would be in excellent agreement. Lifetime broadening should have little effect on the spectra of the low-*Z* members of the series but probably represents the major contribution to the observed L_3 width of Ni since the *d*-band contribution should be only a few tenths of an eV.[17]

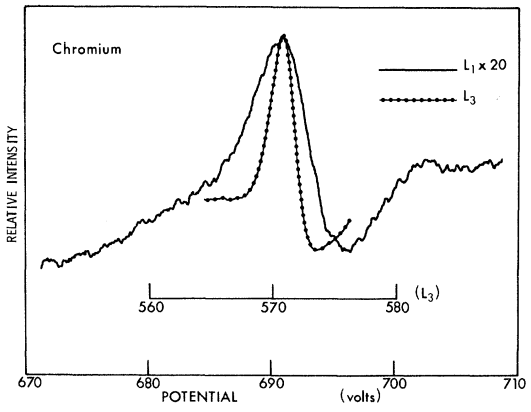

FIG. 15. Comparison of the Cr L_3 and L_1 peaks. The L_3 peak width is due almost entirely to the unoccupied 3*d* states. The L_1 width is due primarily to broadening from the strong $2p \rightarrow 2s$ Coster-Kronig transition.

VI. LIFETIMES OF 2*s* HOLES

Because of the strong $2p \rightarrow 2s$ Coster-Kronig transition, it is expected that the lifetime broadening of the L_1 level will be an order of magnitude greater than for the L_3.[9] This is evident from the comparison of the Cr L_3 and L_1 spectra in Fig. 15. The L_3 width is due almost entirely to the width of the unfilled *d* band, whereas the width of the L_1 peak is about what one would expect due to lifetime broadening alone.[9]

The L_1 peak widths for the entire series are plotted in Fig. 16 along with the lifetimes calculated by McGuire.[9] Although the widths are of the right order of magnitude, the calculated trend toward greater L_1 level widths with increasing *Z* fails

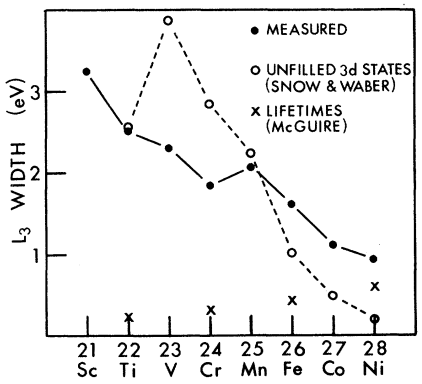

FIG. 14. L_3 peak widths measured at half-maximum and corrected for a 1-eV instrument response function (solid dots), compared with the calculations of Snow and Waber (Ref. 17) for the width of the unfilled 3*d* band (open circles) and the L_3 lifetimes calculated by McGuire (*X*'s) (Ref. 9).

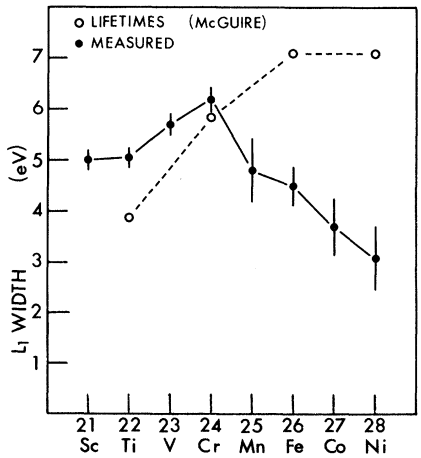

FIG. 16. The L_1 peak widths compared to the lifetime calculations of McGuire (Ref. 9). The order of magnitude is correct, but the decrease for $Z > 24$ is unexpected.

above Cr.

VII. DISCUSSION

Direct quantitative comparisons of our measurements with those obtained by other techniques are possible to only a limited extent, except in the case of the core-level binding energies. The agreement between our values for the L_3-L_2 spin-orbit splittings (Table I) and tabulated x-ray values is reassuring, but of greater interest is the fact that our absolute binding energies (Table II) are in all cases lower than the literature values. Early onsets for the L_3 levels of Co and Ni have also been observed by the characteristic isochromat technique[6,7] which makes essentially the same measurement using an x-ray monochromator rather than potential modulation to reduce the effect of the bremsstrahlung background. Dev and Brinkman[7] point out that this is to be expected since the electron penetration depth is very small and the reduced coordination of the surface atoms should produce a "chemical" shift in their core electrons to lower binding energies.

The same considerations must, of course, apply to x-ray photoelectron measurements of the core levels. For Mg K_α or Al K_α excitation, the escape depth for L-shell electrons of the $3d$ metals should be about the same as the excitation depth in the appearance-potential technique. Unfortunately, researchers in photoelectron spectroscopy have rather uncritically accepted estimates of an effective sampling depth of about 100 Å.[18] Steinhardt, Hudis, and Perlman,[19] however, have recently shown using electron spectroscopy for chemical analysis (ESCA) that 1000-eV electrons have an escape depth of only about 10 Å in graphite, and it would presumably be even less for the more dense $3d$ metals. This agrees with what one would expect from theoretical considerations,[20,21] and from a great body of experimental low-energy-electron-diffraction (LEED) observations.

Because it was assumed that the escape depth was far greater than this, most of the published (ESCA) measurements were taken on surfaces whose cleanliness is open to question. Indeed, to date, relatively few ESCA measurements have been made under the ultraclean conditions that characterize modern surface research. Thus, recent compilations of core-level binding energies which have relied heavily on ESCA measurements for reference levels[14] should be viewed with some skepticism, not only because of questions of cleanliness but also the more basic question of whether electron-binding energies measured by surface-sensitive techniques are representative of bulk properties of matter.

For most of the other measurements reported here, such as peak widths, we can make no direct experimental comparisons, but must instead look to band-structure calculations at the one extreme which claim validity only for the bulk and at the other extreme, calculations based on the ground-state configuration of free atoms. The systematic changes in the $2p$ spectra with Z are, nevertheless, in reasonable accord with a rigid-band model of the transition metals. In particular, the threshold-peak width, which is a measure of the unfilled width of the $3d$ band, decreases with Z. It would be expected on this basis that the $2p$ spectra of Cu, for which the $3d$ band is filled, would exhibit simple steps at the L_3 and L_2 thresholds rather than the distinctive peaks of the transition metals, and preliminary studies of Cu show that this is indeed the case.

The corresponding behavior for a filled-band probe such as ESCA would be an increase in the width of the $3d$ peak with Z. While no systematic ESCA study of the entire $3d$ series is known to the authors, valence-band ESCA spectra of Fe, Co, and Ni have been published by two different groups.[22,23] These spectra appear to follow the reverse of the expected trend, that is, the width of the peak associated with the filled $3d$ band decreases with Z over this limited range.

The treatment of the spectral line shapes solely in terms of the density of states is, of course, an oversimplification. The measured spectra must depend, to some unknown extent, on the oscillator strengths as well as on many-electron effects. Threshold singularities due to the interaction of the core hole with low-lying, single-particle excitations of the conduction electrons are frequently reported in x-ray emission and absorption, and Laramore[24] has shown that it is possible for even stronger threshold divergencies to occur in appearance-potential spectroscopy. Indeed, the graphite K excitation appears to be dominated by a resonant coupling to the plasmon spectrum.[25–27] There is, however, no evidence of these many-electron effects in the results presented here. The extended fine structure observed above the L_3, L_2 thresholds, particularly for Ni, probably consists of characteristic loss replicas of the main peaks.[16]

The most intriguing anomalies reported here are the variation of the L_3/L_2 intensity ratios and the L_1 lifetimes with Z (Fig. 11). In both cases, the Z dependence for $Z \leq 24$ is just the opposite of that for $Z \geq 24$. $Z = 24$ (Cr) corresponds to the case in which the $3d$ band is just half-filled. The cohesion of the transition metals exhibits a similar variation with the filling of the d band, increasing through the first half of the series as predominantly bonding states are filled, and decreasing thereafter as antibonding states are occupied.[28] It seems likely that the variation in radiative-transition rates re-

flects the same changes in electronic structure that are responsible for the variation in cohesive energy.

ACKNOWLEDGMENTS

We wish to acknowledge many helpful discussions with E. J. McGuire and G. E. Laramore. In addition, we would like to acknowledge the expert technical and computer-programming assistance of D. G. Schreiner without which the present work would have been considerably delayed.

*Work supported by the U. S. Atomic Energy Commission.

[1]H. W. Skinner, T. C. Bullen, and J. E. Johnston, Phil. Mag. 45, 1070 (1954).

[2]V. A. Fomichev, A. V. Rudnev, and S. A. Nemnonov, Fiz. Tverd. Tela 13, 1234 (1971) [Sov. Phys. Solid State 13, 1031 (1971)].

[3]D. E. Eastman, J. Appl. Phys. 40, 1387 (1969); Solid State Commun. 7, 1697 (1969).

[4]R. L. Park and J. E. Houston, Surface Sci. 26, 664 (1971).

[5]R. J. Liefeld, in *Soft X-Ray Band Spectra*, edited by D. J. Fabian (Academic, New York, 1968).

[6]A. F. Burr, Adv. X-Ray Anal. 13, 426 (1969).

[7]B. Dev and H. Brinkman, Ned. Tijdschr. Vacuumtechn. 8, 176 (1970).

[8]Marz-grade purity obtained from Materials Research, Inc., Orangeburg, N. J.

[9]E. J. McGuire (unpublished).

[10]J. A. Bearden and A. F. Burr, *Atomic Energy Levels* (U. S. Atomic Energy Commission, NYO 2543-1, Oak Ridge, Tenn. 1965).

[11]H. Merz, Phys. Status Solidi 1, 707 (1970).

[12]W. B. Nottingham, Phys. Rev. 47, 806(A) (1935).

[13]M. Siegbahn, in *Spektroskopie der Röntgenstrahlen* (Springer, Berlin, 1931).

[14]J. A. Bearden and A. F. Burr, Rev. Mod. Phys. 39, 125 (1967).

[15]J. E. Houston and R. L. Park, Phys. Rev. B 5, 3808 (1972).

[16]J. E. Houston and R. L. Park, J. Chem. Phys. 55, 4601 (1971).

[17]E. C. Snow and J. T. Waber, Acta Met. 17, 623 (1969).

[18]K. Siegbahn *et al.*, *ESCA* (Almqvist and Wiksells Boktryckeri AB, Uppsala, 1967).

[19]R. G. Steinhardt, J. Hudis, and M. L. Perlman, Phys. Rev. B 5, 1016 (1972).

[20]J. J. Quinn, Phys. Rev. 126, 1453 (1962).

[21]L. Kleinman, Phys. Rev. B 3, 2982 (1971).

[22]C. S. Fadley and D. A. Shirley, Phys. Rev. Letters 21, 980 (1968).

[23]Y. Baer, P. F. Hedman, M. Klasson, C. Nordling, and K. Siegbahn, Physica Scripta 1, 55 (1970).

[24]G. E. Laramore, Phys. Rev. Letters 27, 1050 (1971).

[25]D. C. Langreth, Phys. Rev. Letters 26, 1229 (1971).

[26]J. E. Houston and R. L. Park, Solid State Commun. 10, 91 (1972).

[27]G. E. Laramore, Solid State Commun. 10, 85 (1972).

[28]See for example J. Friedel, in *The Physics of Metals 1. Electrons*, edited by J. M. Ziman (Cambridge U. P., Cambridge, England, 1969), p. 340; L. Brewer, Science 161, 115 (1968).

PHYSICAL REVIEW B VOLUME 6, NUMBER 4 15 AUGUST 1972

Quantum Crystals in the Single-Particle Picture

Laurent G. Caron*

Jet Propulsion Laboratory, California Institute of Technology, Pasadena, California 91103

(Received 28 February 1972)

A low-temperature formalism for quantum crystals based on the localized-single-particle picture is presented. A proposed transcription to a quasiparticle space provides the basis for an easily accessible thermal analysis. It also yields correlation and lifetime information. The excitations are shown to be the same as Werthamer's. The effect of wave-function overlap and its impact on magnetism are also discussed. Lastly, the defect crystal is examined.

I. INTRODUCTION

The breakdown of classical phonon theory in quantum crystals has resulted in recent efforts being channeled in either a single-particle or a collective approach.[1] The phonon spectra in both pictures show striking similarities. It should then be possible, in principle, to use either representation to get at the low-temperature thermodynamics of quantum crystals. One difficulty with the single-particle representation has been in determining this low-temperature behavior from a knowledge of the excitation spectrum. It is the purpose of this paper to present a low-temperature formalism of the random-phase-approximation (RPA) phonons that will be amenable to overlap and defect analysis.

The procedure, reminiscent of the one in spin-wave theory, involves mapping the atomic eigenvector space into a boson space. The imaged Hamiltonian, under a proposed set of transformation rules, can be transformed to yield the ground-state